Basic mechanisms of DBS for Parkinson's disease: computational and experimental studies on neural dynamics

Çağnan, H.

Publication date
2010

Chapter 3

From parkinsonian thalamic activity to restoring thalamic relay by Deep Brain Stimulation: new insights from computational modeling

Authors

Hil G.E. Meijer, Martin Krupa, Hayriye Cagnan, Marcel A.J. Lourens, Tjitske Heida, Hubert C.F. Martens, Lo J. Bour and Stephan A. van Gils

Based on the paper under review

Abstract

This study presents a computational model of a thalamocortical relay (TCR) neuron that is used to explore thalamic relay fidelity in relation to Parkinson's disease (PD) and Deep Brain Stimulation (DBS). Several experimental studies demonstrated the oscillatory interaction within and between the Basal Ganglia nuclei accompanied with a strong tendency to synchronization in the theta (3.5-7 Hz) and beta (13-30 Hz) frequency bands. These oscillations have a profound influence on TCR neurons and impair relay of excitatory cortical inputs by inducing rebound action potential generation. In the resting state, without additional sensorimotor input, rebound activity is generated for even mild inhibition from the globus pallidus internum (GPi). Periodic input corresponding to high frequency DBS is found to suppress this activity for mild and even more prominent GPi inhibition when stimulation amplitude and frequency are chosen within a specific stimulation window. While the low frequency rebound activity hinders relay of excitatory cortical inputs by the TCR neuron, high frequency stimulation with parameter settings corresponding to this specific window restores the relay functionality.

3.1 Introduction

Parkinson's disease (PD), a neurodegenerative movement disorder, is accompanied with synchronous oscillatory activity patterns at multiple levels of the basal ganglia-thalamocortical loop (Hammond et al. 2007). Primary motor symptoms are tremor at rest, bradykinesia, akinesia, and rigidity. When medication is no longer effective, Deep Brain Stimulation (DBS) can be applied at the subthalamic nucleus (STN) (Hashimoto et al. 2003, Levy et al. 2000), the globus pallidus internum (GPi) (Anderson et al. 2003), or the ventral intermediate thalamic (VIM) nucleus (Benabid et al. 1991) to suppress disease symptoms. While thalamic DBS mainly reduces tremor, DBS applied at the STN or the GPi predominantly alleviates other PD motor symptoms, including rigidity and bradykinesia. In a five-year prospective study of 49 patients treated with bilateral STN stimulation, an average improvement at five years for motor function while off medication as compared with baseline was 54% ($p<0.001$) and those for activities of daily living improved by 49% ($p<0.001$) (Krack et al. 2003). It is remarkable that irrespective of the target nucleus (i.e. STN, GPi, VIM), DBS was found to be effective only for very specific parameter ranges, most notably for high frequency (>100 Hz) and relatively low stimulus intensity (Moro et al. 2002). Parameter settings for DBS are based on several studies (Benabid et al. 1991; Limousin et al. 1995; Volkmann et al. 2002; Volkmann et al. 2006). Despite high clinical success, the mechanism by which DBS suppresses or modulates away from pathophysiology of the motor network remains unknown. Several hypotheses have been formulated regarding mechanism of DBS, including depolarization blockade, synaptic inhibition, synaptic depression and stimulation-induced disruption of pathological network activity (McIntyre et al. 2004).

Pathophysiology of PD is characterized by increased firing rates of neurons in several Basal Ganglia (BG) nuclei (e.g. STN and GPi) together with a tendency towards bursting and abnormal synchronization in the basal ganglia-thalamocortical loop (Brown 2003). Numerous experimental studies linked synchronization at frequencies within the theta (3.5-7 Hz) and beta (13-30 Hz) frequency bands in the basal ganglia-thalamocortical loop to PD motor symptoms (Brown 2003; Chen et al. 2007; Trottenberg et al. 2007). In this circuit the thalamus is at a key position as it receives convergent

afferent input from the GPi, the cortex and the peripheral system and projects back to the cortex including motor areas (Smith et al. 1998).

Thalamocortical relay (TCR) neurons exhibit oscillatory bursting patterns upon release from hyperpolarization. The ionic mechanism underlying this rebound behavior is the slow, low-threshold T-type Ca^{2+} current. It was reported that during DBS the output of the BG as received by thalamus is modulated rather than restored to a normal state (Dostrovsky and Lozano 2002; Hashimoto et al. 2003; Rubin and Terman 2004). Therefore, the response of TCR neurons to inhibitory input from the BG output nucleus, GPi, under both PD and DBS conditions seems vital for our understanding of the DBS mechanism(s). In their pioneering work, Rubin and Terman (2004) have given strong indications to why STN-DBS induced synchronized BG output at high frequencies (i.e. around 167 Hz) restores the thalamic relay of excitatory input, while oscillatory input, synchronized in the theta and band frequency bands from the BG, impairs this function (Rubin and Terman 2004). In a later study, they have used a computational model of a single TCR neuron as well as a heterogeneous population of TCR neurons to determine thalamic relay fidelity both with simulated BG output and with experimentally recorded GPi spike trains from normal control and MPTP treated monkeys (Guo et al. 2008). For both the theoretical and experimentally recorded GPi activity used as input to the TCR neuron model, similar conclusions could be drawn regarding loss of thalamic relay fidelity during PD (Guo et al. 2008).

In chapter 2, we studied how STN-DBS parameters modulate output of a TCR neuron and observed an inverse relationship between DBS frequency and amplitude required to suppress relay of synchronized BG oscillations to cortex. In this study, we investigate TCR membrane properties and modulation of TCR output in further detail, using a single compartment TCR neuron model. First, we study the neuron's membrane properties using numerical bifurcation analysis. Next, we explore input amplitude and frequency dependency in the generation and suppression of rebound activity, complementary to the work of Rubin and Terman (2004). The TCR neuron model is also used to investigate possible mechanisms underlying the existence of a clinically effective stimulation window, i.e. low stimulation amplitude and high

frequency. To this end, we study how stimulation frequency and amplitude modulates relay of low frequency oscillatory BG and excitatory cortical inputs and identify a stimulation parameter window where relay of low frequency oscillatory BG input is suppressed while relay of excitatory cortical input is preserved.

3.2 Methods

In this study, the following assumptions were made: 1) Synchronized oscillatory activity patterns associated with PD motor symptoms are assumed to remain partially present in BG output during DBS in accordance with clinical observations that firing patterns of some STN neurons appear unaltered during DBS with standard settings (Carlson et al. 2010) and that PD symptoms prevail during sub-therapeutic DBS (Butson and McIntyre 2005; Hashimoto et al. 2003; Moro et al. 2002; Rizzone et al. 2001). We assume that synchronized oscillatory activity patterns persist, as stimulation might affect only part of the stimulated nucleus and corresponding pathways in the BG (Johnson and McIntyre 2008). 2) We assume that DBS-induced high frequency patterns are transmitted through the BG network and give rise to a tonic high frequency synaptic input to the thalamus through GPi (Lozano et al. 2002). In chapter 2, for STN-DBS, we have shown that DBS frequency is transmitted via the GPi output in a computational model of a BG network.

3.2.1 The thalamocortical relay neuron model

The TCR neuron is represented by a single compartment model with membrane dynamics based on earlier modeling work (Cagnan et al. 2009; McIntyre et al. 2004) and neurophysiological data (Destexhe et al. 1998; Huguenard and McCormick 1992; McCormick and Huguenard 1992). From experimental studies it can be concluded that highest T-type Ca^{2+} channel densities are found in the distal dendrites (dendritic region at > 11 μm from the soma). Without including dendritic compartments, T-type Ca^{2+} channel behavior can be included in the single compartment model under the constraint that its I-V curves are similar to those of intact cells (Destexhe et al. 1998). In this way, the model enables the generation of low-threshold bursts, in line with experimental recordings. The time-derivative of the membrane potential (V) of the TCR neuron, the gating variables and Ca^{2+} concentration are given by

$$\begin{aligned} C\,{}^{dV}\!/_{dt} &= -(I_{Na,t} + I_{K,DR} + I_{K,s} + I_T + I_h + I_{Na,leak} \\ &\quad + I_{K,leak} + I_{GPi,Th} + I_{Ctx,Th}) \\ {}^{dX}\!/_{dt} &= (X_\infty - X)/\tau_X \end{aligned} \tag{1}$$

$$d[Ca]_i/_{dt} = ([Ca]_{buf} - [Ca]_i)/\tau_{Ca} - k_{Ca}I_T$$

Here $I_{Na,leak}$ and $I_{K,leak}$ represent sodium and potassium leak currents, respectively, $I_{K,DR}$ fast and $I_{K,s}$ slow potassium currents, $I_{Na,t}$ is a transient sodium current, I_T is a low-threshold T-type Ca^{2+} current, I_h a hyperpolarization-activated current. The synaptic input the TCR neuron receives from the GPi is described by $I_{GPi,Th}$ and excitatory input from the cortex is described by $I_{Ctx,Th}$. Gating variables $X \in \{m, k, n, m_T, h_T, c, d, e_1, e_2\}$ satisfy first order differential equations. Steady states (X_∞) and time constants (τ_X) of the gating variables are described in the Appendix (currents are expressed in mA/cm^2, conductances in mS/cm^2, time in ms, voltages in mV, and ion concentrations in mM).

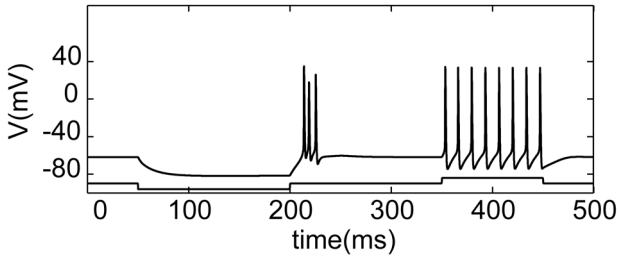

Figure 1: Response of the TCR neuron model to input currents. Upon release from a hyperpolarizing input current (2 mA/cm^2 applied for 150 ms starting at t = 50 ms), a rebound burst appears, while the neuron fires tonically in response to a depolarizing input (2 mA/cm^2 for 100 ms starting at t = 350 ms).

In the absence of input from the GPi or the cortex, the TCR neuron is at rest at approximately -60 mV. Application of depolarizing current, results in tonic spiking (Fig. 1). The TCR neuron responds with a train of action potentials as it is released from inhibition, i.e. rebound burst (Fig. 1) (Destexhe and Sejnowski 2003; Sherman 2001; Smith et al. 2000). T-type Ca^{2+} channels play an important role in the generation of rebound action potentials. In particular, T-inactivation variable h_T de-inactivates when the neuron receives inhibitory input. Upon release from inhibition the membrane potential repolarizes to the resting membrane potential. T-activation gate m_T acts on a much shorter time-scale than h_T and for a limited time window the T-type Ca^{2+} channels will be open. This Ca^{2+} current depolarizes the neuron and

rebound spikes are observed until h_T is again inactivated thereby decreasing the T-type Ca^{2+} current.

3.2.2 Inputs to the thalamocortical relay neuron model

a) Spike pattern derived from GPi-MER

Micro-electrode recordings (MER) obtained from a single PD patient who underwent DBS electrode implantation in the GPi was retrieved. The procedure for DBS was a one stage bilateral stereotactic approach, using frame-based three-dimensional MRI reconstructions for target calculations and path-planning, with MER and macro test stimulation. The standard target coordinates used were 21 mm lateral to the midplane, 2 mm anterior to the midcommissural point (MCP) and 5 mm below the intercommissural point (ICL) for the GPi. The patient was awake during the surgical procedure and was not under the influence of any sedatives. Surgery and MER were performed following overnight withdrawal from anti-parkinsonian (i.e. Levodopa) medication. Extracellular single/multi-unit MER was performed with small (10 μm width) polyamide-coated tungsten microelectrodes (Medtronic microelectrode 291; impedance ≈ 1.1 MΩ measured at 220 Hz at the beginning of each trajectory) mounted on a sliding cannula. Signals were recorded with the amplifiers (10,000 times amplification) of the Leadpoint system (Medtronic), using a bootstrapping principle and were analog band-pass filtered between 500 and 5000 Hz. The signal was sampled at 12 kHz, by use of a 16-bit A/D converter and afterwards up-sampled to 24 kHz off-line. Following a signal stabilization period of two seconds after electrode movement cessation, multi-unit segments were recorded for 5-40 seconds. Starting from 12 mm above the MRI-based target, microelectrodes were advanced in steps of 500 μm towards the target by a manually controlled microdrive. At each depth, the spiking activity of the neurons lying close to the needle (an area with a radius up to about 200 μm) could be recorded. Depending on the neuronal density, not more than 3-5 units were recorded simultaneously. More distant units could not be distinguished from the background noise. Based on surgical annotations made by expert neurophysiologists during DBS electrode implantation, an MER trajectory was selected. Spikes were identified using the envelope method (Dolan et al. 2009) and

spike sorting was performed in order to extract the spike pattern used as input to the TCR neuron. The spectrum of the signal was then calculated according to Halliday et al. (1995) and showed a strong frequency component near 5 Hz, see figure 2B.

b) GPi input

The GABAergic GPi input is described using

$$I_{GPi,Th} = (g_{PD}s_{PD}(t) + g_{DBS}s_{DBS}(t))(V - E_{GABA}) \quad (2)$$

The post-synaptic conductance changes, $s_{PD}(t)$ and $s_{DBS}(t)$, are modeled as impulse responses that decay exponentially with time constant $\tau_{GABA} = 10$ ms. $s_{PD}(t) = \exp(-(t - t_i)/\tau_{GABA})$, where t_i is equivalent to the most recent GPi spike time. GPi spike times were derived from the GPi-MER, as described in the preceding section and shown in figures 2A and 4B. Average bursting frequency of the GPi neuron was 5 Hz (Fig. 2B).

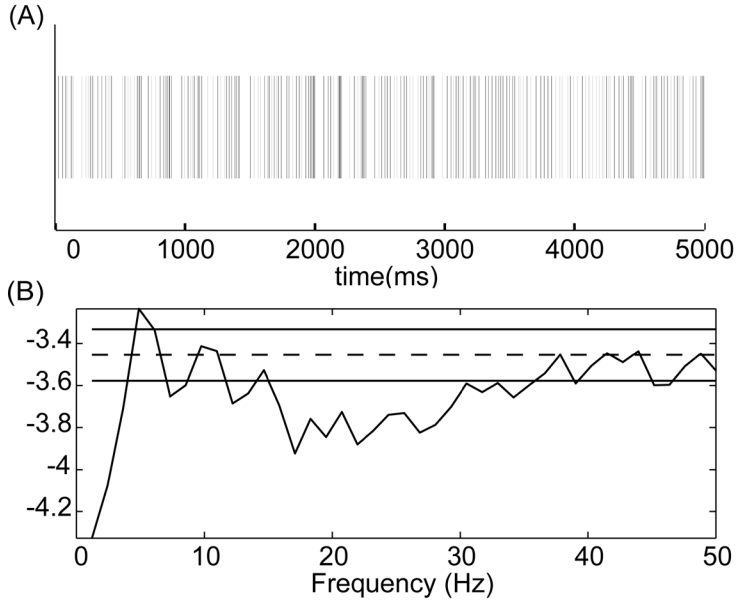

Figure 2: A: First 5 seconds of the experimental GPi time series. B: Spectrum of the experimental GPi time series. 95% confidence levels are indicated by dashed lines.

The post-synaptic conductance change induced by DBS (second term in Eq. 2) is modeled as a periodic exponentially decaying pulse train $s_{DBS}(t) = \exp(-\mathrm{mod}(t, 1000/f_{DBS})/\tau_{GABA})$, where mod is the modulus function. Parameters g_{PD} and g_{DBS} represent maximum conductances. During DBS, activity at the target nucleus is assumed to be partially overwritten depending on the volume of tissue activated, based on previous computational studies (Butson and McIntyre 2005; Hahn and McIntyre 2010). In order to ensure that average inhibition applied to the TCR neuron remains constant, we keep the sum of g_{PD} and g_{DBS} constant by setting $g_{PD} = g_{PD,max}(1-\lambda)$ and $g_{DBS} = \beta g_{PD,max}\lambda$. The recruitment factor λ (between 0 and 1) represents fraction of the GPi input that is replaced with tonic DBS induced activity patterns. β accounts for an increase in firing rate due to electrical stimulation (Hahn et al. 2008; Reese et al. 2008) and ranges from 1 to 2. Finally, we set $E_{GABA} = -85$ mV (McIntyre et al. 2004; Rubin and Terman 2004).

The spike pattern derived from GPi-MER exhibits average bursting frequency of 5 Hz. In order to perform a thorough analysis on the response of the TCR neuron to the complete frequency range associated with parkinsonian oscillatory activity, we make use of a simulated GPi input. This reduced representation was previously described in chapter 2.

$$I_{GPi,Th} = g_{GPi,Th}\big(1 + \alpha_P sin(2\pi f_P t)\big)(V - E_{GABA}) \qquad (3)$$

The GPi input is characterized by an oscillation frequency f_P which represents the average bursting frequency of the pre-synaptic GPi neurons. α_P is the modulation depth that gives a measure of the synchronization level among the pre-synaptic GPi neurons; its value ranges between 0 (i.e. uncorrelated) and 1 (i.e. complete synchronization). For equation 3 we set $g_{PD,max} = g_{GPi,Th}(1+\alpha_P)$.

c) Sensorimotor input

The excitatory (glutamatergic) synaptic input from the cortex, $I_{Ctx,Th}$, is modeled as a sequence of block pulses $s_{Ctx,Th}(t)$ with a pulse width of 5 ms ($s_{Ctx,Th} = 1$ during the pulse and $s_{Ctx,Th} = 0$ otherwise) and pulse amplitude of $g_{Ctx,Th}$ (Rubin & Terman 2004, Guo et al. 2008)

$$I_{Ctx,Th} = g_{Ctx,Th}\, s_{Ctx,Th}(t)(V - E_{Glut}) \qquad (4)$$

The reversal potential for glutamate is $E_{Glut} = 0$ mV (Destexhe et al. 1998; Kim et al. 1997; McIntyre et al. 2004; Rubin and Terman 2004; Terman et al. 2002).

3.2.3 Simulation protocol

Analysis of the TCR neuron model was performed using the MATLAB toolbox MATCONT, a continuation and bifurcation toolbox for the interactive numerical study of dynamical systems (Dhooge et al. 2003). Periodic orbits have been computed using 80 mesh points and standard tolerances. Time signals were computed using MATLAB (version 7.3, The MathWorks, Inc.) using "ode15s" for solving the differential equations.

a) TCR response to GPi input

First, we investigate the response of the TCR neuron to GPi input only, i.e. without high frequency stimulation and sensorimotor input ($g_{DBS} = g_{Ctx,Th} = 0$ mS/cm^2). First, we increase $g_{PD,max}$ to a value where the low frequency oscillations observed in the experimental GPi time series elicit rebound responses. Subsequently, we consider the sensitivity of our results to the level of synchrony and average burst frequency of pre-synaptic GPi neurons using equation 3. We vary the parameters of the synaptic input $g_{GPi,Th}$, f_P, and α_P. Initially f_P in equation 3 is set to 8 Hz and $g_{GPi,Th} = 0.1$ mS/cm^2. When we increase α_P, there is a critical value α_{c1} indicating the threshold between the generation of sub-threshold oscillations and rebound spikes. Reversing the direction, starting at $\alpha_P = 1$ and decreasing α_P, we find another value α_{c2} indicating a threshold between the generation of rebound spikes and sub-threshold oscillations. Both thresholds α_{c1} and α_{c2} are detected automatically within MATCONT. We have determined both critical values while varying f_P.

b) Stimulation induced patterns: rebound suppression and relay reliability

By applying a stimulation signal we investigate if, how, and under which conditions application of high frequency inhibitory input prevents the TCR neuron from responding to and relaying the bursting GPi input. Here we only use the

experimentally recorded GPi time series (Eq. 2). To analyze the performance of stimulation in suppressing rebound responses we define the suppression level S as the ratio of the number of suppressed rebound spikes and the number of rebound spikes without stimulation. When a rebound response consists of multiple spikes, it is counted as one response. In the presence of cortical excitatory input, the relay function of the TCR neuron is tested using the relay level R defined as the ratio of successfully relayed input pulses and the number of excitatory pulses. Based on the excitatory input, the expected spike times are known and therefore we can classify the generating mechanism for each action potential. We distinguish between relay of excitatory input pulses and rebound responses to inhibitory bursting GPi input. Suppression and relay levels allow investigating separately the two different responses that may be attributed to pathology, i.e. the inability to relay sensorimotor signals, and the generation of rebound responses, resulting in transmission of the BG oscillatory content to cortex. $S > 0.9$ is considered to indicate sufficient rebound suppression and $R > 0.9$ to indicate sufficient relay. Simulations are performed for stimulation frequencies up to 200 Hz (starting at 20 Hz with steps of around 15 Hz) with λ, the level of overwriting, between 0 and 1 (with an average step size of 0.05). We use $g_{PD,max} = 0.4\ \mathrm{mS/cm^2}$ and test $\beta = 1.0,1.2,1.5,2.0$. For the excitatory input level we use $g_{Ctx,Th} = 0.13,0.15,0.17\ \mathrm{mS/cm^2}$ Lower values of $g_{Ctx,Th}$ lead to insufficient relay, while for values larger than 0.2 each excitatory input yields two spikes which is also classified as bad relay. The timing of the excitatory pulses is determined according to a Poisson distribution with a mean frequency of 16.5 Hz. In order to test the sensitivity of the model neuron, we increase the maximum T-type Ca^{2+} channel permeability level, p_{Ca}, corresponding to the strength of the T-type Ca^{2+} current, from 0.1 to 0.15 cm/s. Simulation of each of the conditions spans a period of 40 s.

3.3 Results

3.3.1 Response of the TCR neuron to GPi input

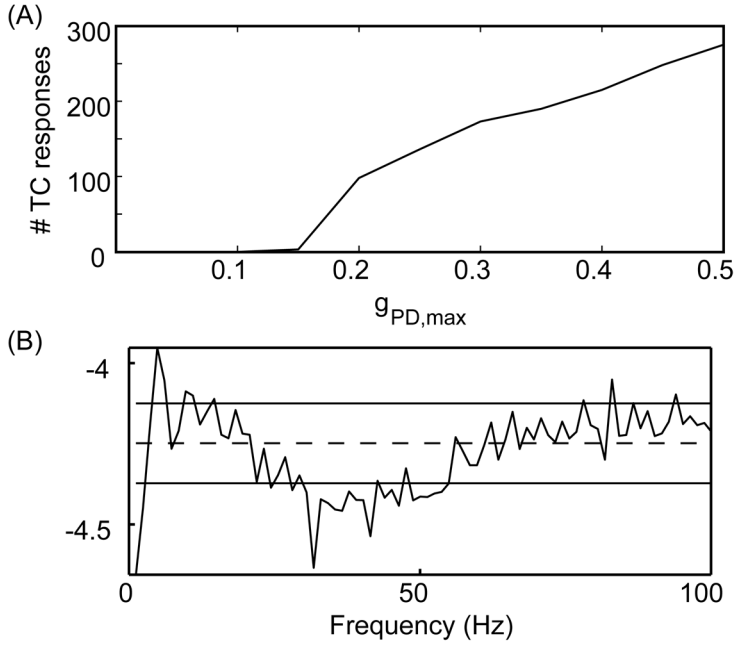

Figure 3: Response of the TCR neuron to GPi input. A: Number of rebound responses as a function of $g_{PD,max}$. For $g_{PD,max} >$ 0.35 mS/cm^2 some rebound responses consist of multiple spikes. B: Spectrum of the TCR response with peaks around 5 and 90 Hz for $g_{PD,max} = 0.5$ mS/cm^2. The first peak is due to the GPi burst frequency, the second peak is due to bursts consisting of multiple spikes.

We simulated the TCR response to the spike pattern derived from the GPi-MER, according to equation 2. Average GPi bursting frequency was 5 Hz (Fig. 2B). We tested the effect of $g_{PD,max}$ (i.e. strength of the GPi input) on the TCR response by increasing $g_{PD,max}$ from 0 to 0.5 mS/cm^2 in the absence of DBS-driven and excitatory cortical input (i.e. $g_{DBS} = g_{Ctx,Th} =$ 0 mS/cm^2). For small $g_{PD,max}$ there is only sub-threshold TCR activity, while above a threshold of $g_{PD,max} \approx 0.15$ mS/cm^2 the TCR neuron shows rebound activity (Fig. 3). We observe that for sufficiently high $g_{PD,max}$, spiking frequency of the TCR neuron is 5 Hz (Fig. 3B). We conclude that the TCR neuron relays the low frequency component of the GPi input

corresponding to the average GPi bursting frequency (Fig. 2B). The rebound responses of the TCR neuron occur during silent intervals following a GPi burst, see figures 4A-D. During a GPi burst, the T-type Ca^{2+} current de-inactivates providing the depolarizing drive for a post-inhibitory spike. The rate at which the T-type Ca^{2+} current de-inactivates plays a crucial role in determining whether the TCR neuron will spike following a GPi burst e.g. around t=2750 ms (Fig. 4D).

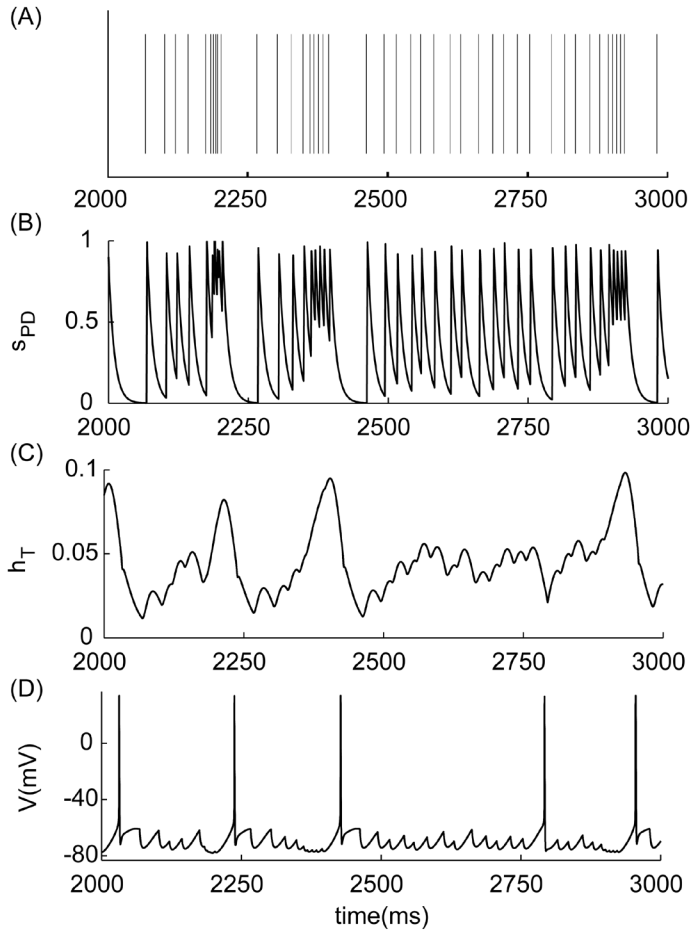

Figure 4: A: the pre-synaptic GPi spike times; B: the synaptic input s_{PD}; C: T-type Ca^{2+} current inactivation gating variable h_T ; D: the membrane potential V of the TCR neuron. ($g_{PD,\max} = 0.3\ \mathrm{mS/cm^2}$, $g_{DBS} = g_{Ctx,Th} = 0\ \mathrm{mS/cm^2}$)

Previous experimental studies indicated that a group of GPi neurons project onto a TCR neuron (Smith et al. 1998). Moreover, it has been reported that GPi neurons in addition to exhibiting bursting activity patterns, are also synchronized to each other in the theta and beta frequency bands during PD (Raz et al. 2000). Therefore, as well as testing the response of the TCR neuron to the strength of the GPi input (Fig. 3), we tested its response to average burst frequency and synchrony of a group of pre-synaptic GPi neurons. In chapter 2, we have shown that the post-synaptic change induced by a group of GPi neurons can be approximated with a sinusoid. Frequency of the sinusoid (f_P) captures the average bursting frequency of the pre-synaptic GPi neurons while the modulation depth (α_P) of the sinusoidal input captures the level of synchrony between the pre-synaptic GPi neurons. Initially f_P in equation 3 is set to 8 Hz and $g_{GPi,Th} = 0.1$ mS/cm^2. When $\alpha_P = 0$, the GPi input is constant and the TCR neuron responds by settling to a steady state. For small α_P the membrane potential responds with small sub-threshold oscillations. When α_P is incrementally increased from 0 to 1, it is observed that for values of α_P below a critical value, α_{c1}, no rebound action potentials are generated, while above this value the TCR neuron will always fire (at least once per period). By reversing the experiment (i.e. decreasing α_P from 1 to 0 until the rebound action potential disappears) it is found that the critical value α_{c2} is smaller than α_{c1}, indicating a region of bistability. Figure 5 shows both critical values as a function of the average pre-synaptic GPi burst frequency. Figure 5 shows that the frequency selectivity of the TCR neuron model has a large overlap with experimentally observed frequencies related to synchronized activity during PD (Brown 2003; Magill et al. 2000; Magnin et al. 2000; Nini et al. 1995; Raz et al. 2000). For a frequency f_P of 8 Hz, i.e. the frequency for which the threshold level is at a minimum, $\alpha_{c1} = 0.81$ and $\alpha_{c2} = 0.79$. The bistable behavior of the TCR neuron for this situation is presented in figure 6. The instability boundaries of the spiking and non-spiking solutions consist of saddle-node and period-doubling bifurcations. These boundaries depend smoothly on other system parameters (Chow and Hale 1982; Kuznetsov 2004).

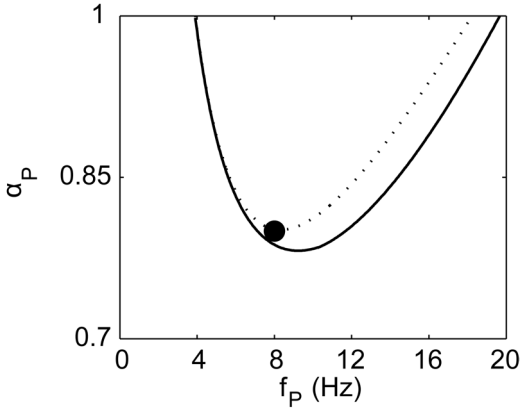

Figure 5: For the frequency range from 3 to 20 Hz the threshold levels for the generation of rebound action potentials (solid line) and no rebound action potentials (dotted line) enclose a region of bistability ($g_{GPi,Th} = 0.1$ mS/cm^2).

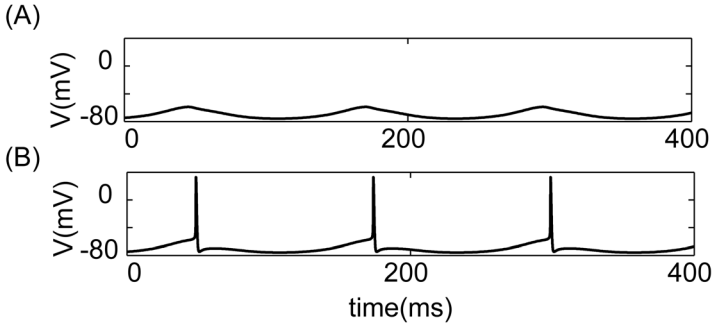

Figure 6: For $f_P = 8$ Hz, $\alpha_P = 0.8$ and $g_{GPi,Th} = 0.1$ mS/cm^2 the TCR neuron described by equation 1 exhibits both A: stable non-spiking and B: stable spiking solutions. This region of bistability ranges from $\alpha_{c2} \approx 0.79 < \alpha_P < \alpha_{c1} \approx 0.81$.

3.3.2 High frequency stimulation: rebound suppression and relay reliability

We investigated modulatory effect of the DBS-driven inhibition from the GPi on the TCR neuron. The TCR neuron received as input the spike pattern derived from the GPi-MER together with the DBS-driven input based on the assumption that DBS does not completely regularize synchronized oscillatory activity patterns observed in the BG during PD (Eq. 2). The addition of stimulation induced inhibitory and excitatory cortical inputs altered the response of the TCR

neuron. Depending on input parameters, several qualitatively different scenarios exist. Examples of these different responses are shown in figure 7 where the membrane potential of the TCR neuron and the excitatory input are presented. For the GPi input we set $g_{PD,max} = 0.4$ mS/cm^2. For the stimulation, we set the frequency $f_{DBS} = 135$ Hz, the rate of activity increment $\beta = 1.2$ and the overwriting parameter λ is low (0.05), intermediate (0.1-0.2) or complete (1.0).

Without excitatory input ($g_{Ctx,Th} = 0$ mS/cm^2) rebound responses still exist during low amplitude DBS (Fig. 7A). For intermediate values of g_{DBS}, these are suppressed due to extra inhibition that keeps the membrane potential below a firing threshold (Fig. 7B). In the presence of excitatory inputs, even at low values of λ, most rebounds are suppressed (Fig. 7C). For intermediate values of λ, rebounds completely disappear (Fig. 7D). Under these conditions, most of the excitatory inputs were relayed. High g_{DBS}, however, induces inhibition causing relay failure (Fig. 7E). Relay failure also occurs if the strength of the excitatory input is too low (Fig. 7F). As soon as stimulation is stopped rebound activity re-appears. Note that only the scenarios shown in figures 7B and 7D seem desirable as both rebounds are suppressed and excitatory inputs are relayed.

Next, we have varied the parameters λ and f_{DBS} systematically to find regions with sufficient rebound suppression ($S > 0.9$) and relay reliability ($R > 0.9$), see figure 8. For each frequency f_{DBS} we have determined a value of the parameter λ corresponding to this threshold resulting in S-curves and R-curves. For all panels rebounds are suppressed above the S-curves and sufficient relay occurs below the R-curves.

For the S-curves (dashed) we distinguish two cases, with and without excitatory input to be relayed, denoted by S_R and S_N, respectively. The S_N-curves shown in figures 8A-F presents the minimal recruitment level (λ) required for a given stimulation frequency f_{DBS} to suppress transmission of the bursting GPi input when no excitatory inputs are applied.

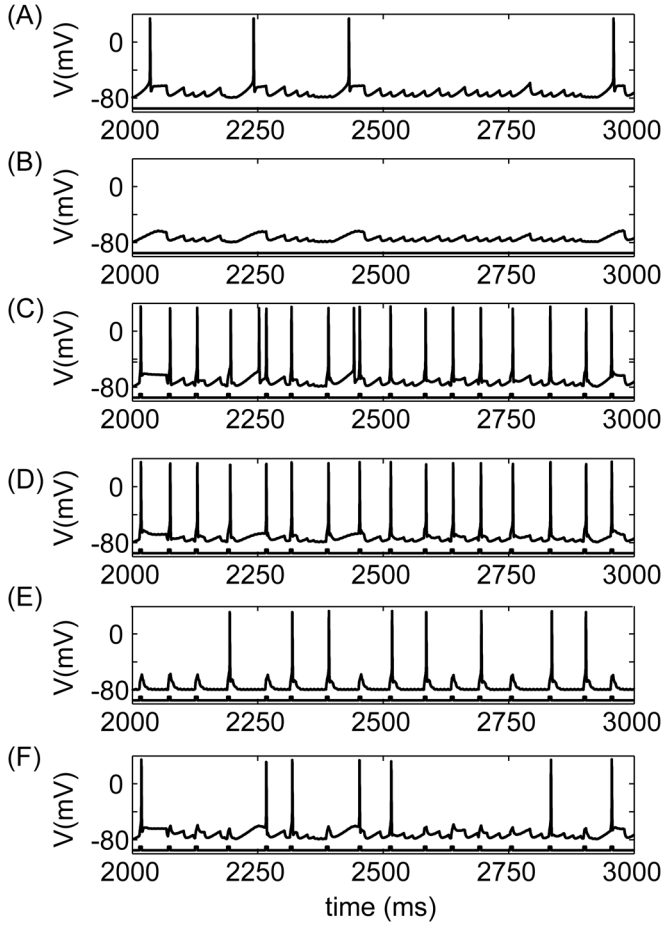

Figure 7: For the GPi input we fix $g_{PD,max} = 0.4\ \mathrm{mS/cm^2}$ and $\beta = 1.2$. The stimulation frequency is set at $f_{DBS} = 135$ Hz. The uppertraces represent the membrane voltage of the TCR neuron. For C-F the precise timing of the excitatory input (mean frequency 16.5 Hz) is displayed beneath each voltage trace. A: $\lambda = 0.05$ and $g_{Ctx,Th} = 0$: DBS too weak; B: $\lambda = 0.2$ and $g_{Ctx,Th} = 0$: DBS sufficiently strong; C: $\lambda = 0.05$ and $g_{Ctx,Th} = 0.15$: DBS too weak, still rebound responses; D: $\lambda = 0.2$ and $g_{Ctx,Th} = 0.15$: Perfect relay and no rebounds; E: $\lambda = 1$ and $g_{Ctx,Th} = 0.15$: relay failure due to strong DBS; F: $\lambda = 0.1$ and $g_{Ctx,Th} = 0.10$: Input too weak.

The S_R-curves have been determined in the presence of excitatory inputs. The S_R-curves are lower than the S_N-curves due to the dynamics of the T-type Ca^{2+} current, in particular the inactivation variable h_T. The excitatory input

($g_{Ctx,Th} = 0.15$ mS/cm^2) gives rise to rapid inactivation of the T-type Ca^{2+} channels thereby preventing a rebound response. As a result, following each GPi burst, the T-type Ca^{2+} current is less de-inactivated in the presence of excitatory inputs. Consequently, after the GPi burst, the stimulation needs to provide less inhibition to prevent the post-inhibitory spike. We conclude that the presence of the excitatory signal enhances the ability to suppress rebounds resulting in substantially lower minimal recruitment levels (λ). This is illustrated in figure 9; for weak DBS and weak excitatory inputs relay failure is observed together with partial rebound suppression.

Both the S_N-curves and S_R-curves show two asymptotes: for frequencies above 100 Hz an almost flat plateau occurs, while for lower stimulation frequencies the minimal recruitment level (λ) increases. Stimulation below 40 Hz fails to suppress rebound activity in most cases. When f_{DBS} is very high (> 150 Hz), the post-synaptic conductance change induced by DBS is nearly constant and the R-curve decreases for increasing f_{DBS}. The combined S_N and R-curves show that certain combinations of stimulation amplitude and frequency, represented by λ and f_{DBS}, respectively, satisfy the condition for both sufficient relay (below R-curve) and rebound suppression (above S_N-curve). Within this amplitude-frequency window, the stimulation prevents transmission of the pathological oscillatory input, but does not impair the relay of excitatory input provided this input is sufficiently strong.

This parameter window ranges for frequencies above 50 Hz and with λ between 0.15 and 0.3. The lower boundary is not demarcated by the S_R-curve as stimulation should also suppress rebounds during rest, i.e. in the absence of excitatory inputs. The size of this amplitude-frequency parameter window varies with altered parameters. First, changing β to 2.0 (Fig. 8B) or 1.2 (Fig. 8C), we see that the R-curve lowers with increasing β. This is expected as the level of inhibition increases and as a result excitatory input is less easily relayed. Increasing β also lowers both S-curves as the stimulation induces more inhibition which makes it easier to suppress rebounds. The effect on the R-curve is much stronger than on the S-curves and for larger β the amplitude-frequency window is smaller.

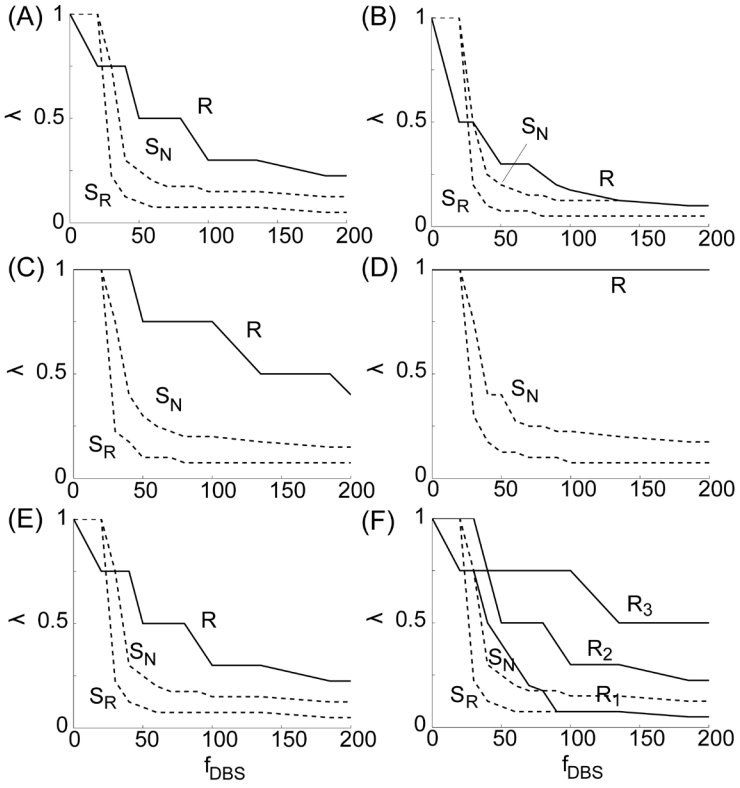

Figure 8: Sufficient suppression occurs above the S-curves (dashed), while sufficient relay is found below the R-curves (solid). For S_N-curves $g_{Ctx,Th} = 0$ mS/cm^2, while for S_R-curves $g_{Ctx,Th}$ is nonzero. Parameters are set to $g_{PD,max} = 0.4$ mS/cm^2, $g_{Ctx,Th} = 0.15$ mS/cm^2 and $p_{Ca} = 0.1$ cm/s unless explicitly specified. A: $\beta = 1.5$, B: $\beta = 2$, C: $\beta = 1.2$, D: $\beta = 1.0$, E: Same as A with stronger T-type Ca^{2+} current (i.e. $p_{Ca} = 0.15$ cm/s), F: different amplitudes for the excitatory input $g_{Ctx,Th} = 0.13$ mS/cm^2 (R_1), 0.15 mS/cm^2 (R_2), 0.17 mS/cm^2 (R_3).

We also see that with $\beta = 1$, i.e. no extra activity due to stimulation, sufficient relay still occurs for $\lambda = 1$, figure 8D. Stronger T-type Ca^{2+} current ($p_{Ca} = 0.15$ cm/s instead of 0.1 cm/s), makes it harder to suppress rebounds raising the S-curves, compare figures 8A and 8E. During an excitatory input, the T-type Ca^{2+} current provides an extra driving force for the relay of the excitatory input, which makes the cell more responsive and raises the R-curve. Third, we see that varying the strength of the excitatory input has a strong effect

on the R-curve, but not the S-curves, figure 8F. This is expected as it mainly influences the chance for successful relay. In fact, the S_R-curve has been plotted for three values of $g_{Ctx,Th}$, but they are nearly indistinguishable.

In case of low cortical input pulse amplitude, the R-curve would overlap with the S_N-curve. In this case, stimulation will not be able to both suppress rebounds and provide sufficient relay. Furthermore, we also tested the effect of different mean frequencies of the excitatory input $f_{Ctx,Th} = 14.5, 16.5, 18.5, 21.5$ Hz (not shown). As $f_{Ctx,Th}$ increases, the R-curve lowers since the probability of DBS-induced inhibition and excitatory pulse overlapping is higher. The effect on the S_R and S_N-curves is negligible.

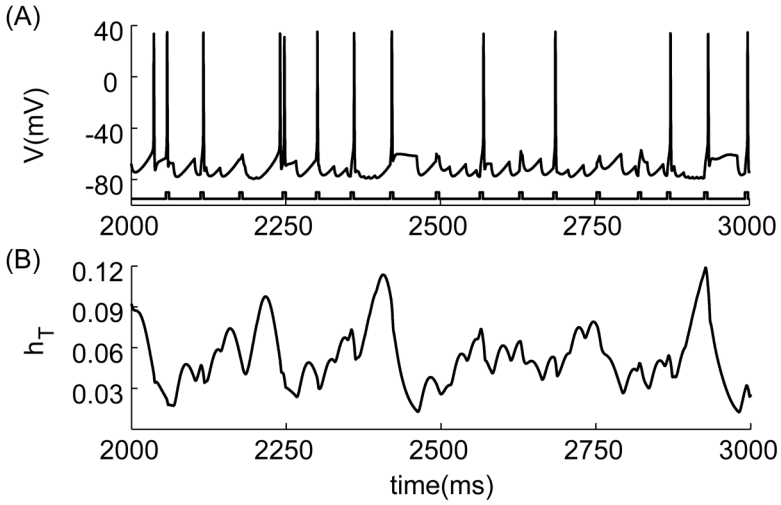

Figure 9: A: membrane potential V and B: h_T with weak input and weak stimulation ($\beta = 1.0$, $\lambda = 0.025$ and $g_{Ctx,Th} = 0.10$ mS/cm^2). The inactivation of the T-type Ca^{2+} current follows the slow oscillation and builds up slowly and decays slowly. During an excitatory pulse the inactivation drops quickly reducing the drive to fire rebounds. Just after a burst there is very little inhibition so that the membrane potential is near its resting potential around -60 mV.

3.4 Discussion

This study investigated modulation of thalamic relay by high frequency stimulation. We have shown that stimulation frequency suppresses relay of low frequency GPi oscillations. Suppression occurs for low stimulation amplitudes, however excessively high amplitudes block relay of excitatory cortical input. Together this yields a parameter window where relay of low frequency oscillatory GPi input is suppressed and relay of excitatory cortical input is preserved. Partial suppression of relay of low frequency GPi oscillations may also be achieved with excitatory input without stimulation.

It has been proposed that two principal modes of synchronized activity within the subthalamo-pallidal-thalamo-cortical circuit exist with the low frequency oscillations (<30 Hz) facilitating slow idling rhythms in the motor areas of the cortex and the high frequency oscillations (>60 Hz) restoring dynamic task-related cortical activity (Brown 2003). Thalamus, which receives convergent GABAergic input from the BG output nucleus, GPi, and projects to the cortex, is located in a unique position in this circuit. Numerical bifurcation analysis revealed that the TCR neuron selectively responds to and relays GABAergic low frequency oscillations (Fig. 5). We observed that the frequency selectivity is an intrinsic property of the membrane (Cagnan et al. 2009). The low frequency response consists of rebound action potentials since the T-type Ca^{2+} current acts as a driving force in generating post-inhibitory action potentials. Qualitative bifurcation theory (Chow and Hale 1982; Kuznetsov 2004) asserts the robustness of the neuron's behavior with respect to perturbations of other system parameters. This frequency dependent response has been reported earlier for thalamic cells by Smith et al. (Coombes et al. 2001; Smith et al. 2001; 2000) who explored the effect of directly injected oscillating current on bursting using a reduced integrate-and-fire model, with input frequencies of 0.1 to 10 Hz. In chapter 2, we have shown that the post-synaptic change induced by a group of synchronized bursting pre-synaptic neurons can be modeled using a sinusoid. Frequency of the sinusoid (f_P) captures the average bursting frequency of the pre-synaptic neurons while the modulation depth (α_P) of the sinusoidal input captures the level of synchrony between the pre-synaptic neurons. In order to perform numerical bifurcation analysis to investigate

selectivity of the TCR neuron to pre-synaptic GPi synchrony and burst frequency, we chose to use the simulated GPi input (Eq. 3, chapter 2) to drive the TCR neuron instead of the GPi-MER, since 1- single MER only captures the spiking pattern of a limited number of neurons (i.e. 3-5 neurons), 2- units captured in a single MER are not necessarily synchronized because proximity does not guarantee synaptic connection between neighboring neurons and neither indicates that neighboring neurons are part of the same functional network, and 3- MERs obtained every 500 μm limits the probability of capturing units which are synchronized to one another. Bifurcation analysis revealed bistable behavior of the TCR neuron, i.e. a non-spiking or silent mode and a rebound spiking mode (Fig. 5). This bistability could lead to a natural fluctuation in the strength of the projection from the thalamus to the cortex.

It was observed that excitatory input was able to suppress rebound activity if the amplitude of the GPi input was not too high. This cortical (excitatory) input may involve sensory information, e.g. visual information for guidance of movement, or preparatory information for the execution of movement, which has been reported to suppress PD tremor (Amirnovin et al. 2004). The presence of excitatory input makes it easier to suppress rebounds. Successful relay of excitatory input disrupts de-inactivation of T-type Ca^{2+} channels which reduces the driving force to generate a rebound spike. This membrane property could contribute to the absence of parkinsonian rest tremor during voluntary movement and to the efficacy of external cues in helping PD patients to execute movements.

Mechanism of DBS has been hypothesized to be complete overwriting and/or regularization of oscillatory synchronized BG activity patterns associated with PD (Kuncel et al. 2007; McIntyre et al. 2004; Rubin and Terman 2004). Rubin and Terman (2004) assumed full overwriting of BG activity during DBS. In this study, regularized GPi activity restored the relay functionality of TCR neurons (Rubin and Terman 2004). Recently, it was shown that full overwriting is not necessary and that there is an inverse relationship between stimulation amplitude and frequency required to suppress relay of BG oscillations (Cagnan et al. 2009). Here, we consider the role of stimulation on TCR function in further detail.

In this study, we consider stimulation to be effective when the generation of rebound activity in response to inhibitory oscillatory input is diminished while the ability to relay cortical information is preserved. As shown in figure 8 successful relay occurs for amplitude-frequency combinations that remain below the R-curves, while for successful suppression of rebound activity amplitude-frequency combinations must be chosen such that they remain above the S-curves. Figure 8 shows that for frequencies below about 40 Hz the stimulation amplitude must be high in comparison to stimulation frequencies above 70 Hz. This is in accordance with the experimentally observed inverse relationship between the DBS frequency and stimulus intensity (Benabid et al. 1991; Gao et al. 1999; Limousin et al. 1995). For low stimulation frequencies, the window created by the R and S-curves is reduced. We hypothesize that the efficacy of high frequency stimulation is embedded in the fact that a regular input of moderate amplitude prevents the relay of bursting GPi input before an informational lesion occurs with increasing amplitude.

We previously used a BG network model projecting on to a TCR neuron to study DBS parameter dependency in suppression of relay of oscillatory synchronized BG activity to cortical regions by the TCR neuron (Cagnan et al. 2009). In this study, we make use of spike patterns derived from GPi-MER and simulated DBS-induced patterns in order to drive the TCR neuron. The reduced input model captures partial overwriting of oscillatory BG activity patterns during DBS through the overwriting parameter λ and the increase in the firing rate of some GPi neurons as a result of the DBS induced activity patterns in the BG network through the parameter β. Experimental and computational studies have shown that regularization and changes in firing rates in the GPi are dependent on STN-DBS frequency (Cagnan et al. 2009; Dorval et al. 2008). It has been reported that STN-DBS gives rise to increased and regularized firing rates at the GPi while low frequency stimulation is not as effective in regularizing GPi oscillatory activity patterns. In this study, β accounts for changes in GPi firing rates independent of DBS frequency.

It should also be noted that pathophysiological changes in PD not only result from changes in firing patterns but also from changes in firing rates and changes in network connections leading to, for example, loss of functional segregation

resulting in interference between competing motor circuits and a reduced ability to suppress unwanted movements (Molnar et al. 2005; Moroney et al. 2008). It may therefore be expected that stimulation acts via different mechanisms on different motor symptoms of PD (Temperli et al. 2003). In support of this hypothesis is the fact that tremor intensity is almost instantaneously reduced when switching on the stimulation, while alleviating bradykinesia, rigidity and axial symptoms requires a longer time scale to take effect (Johnson et al. 2008). The same conclusion can be drawn from the fact that over a 5-year period the effectiveness of DBS is different for different symptoms, as observed by Krack et al. (2003). Worsening of akinesia, speech, postural stability, freezing of gait and cognitive function between the first and the fifth year was found to be consistent with the natural history of PD.

In summary, the mechanism of DBS as explored in this study primarily focuses on the effectiveness of stimulation to suppress relay of oscillatory GPi input. Even though our model is a gross simplification of the output and activity of the combined BG and cortico-thalamic network, the simulation results are in good agreement with experimental data (Benabid et al. 1991; Gao et al. 1999; Limousin et al. 1995). Our results also show that the effectiveness of high frequency DBS may result from selective suppression of relay of oscillations at low frequencies from BG to thalamocortical circuitry, while relay of sensorimotor information is not affected for low stimulation amplitudes. Only at very high stimulation amplitudes (nearly independent of frequency) an 'informational lesion' is observed.

3.5 Appendix

Parameters for the gating variables are represented by $X_\infty = \alpha_X/(\alpha_X + \beta_X)$ and $\tau_X = 1/(\alpha_X + \beta_X)$ (Destexhe et al. 1998; Huguenard and McCormick 1992; McCormick and Huguenard 1992; McIntyre et al. 2004).

Sodium current

$I_{Na} = g_{Na} m^3 h (V - E_{Na})$

$\alpha_m = 0.32\big(-(V_m + 55)\big)/\big[e^{-(V_m+55)/4} - 1\big]$

$\beta_m = 0.28(V_m + 28)\,/\big[e^{(V_m+28)/5} - 1\big]$

$\alpha_h = 0.128e^{-(V_m+51)/18}$

$\beta_h = 4\,/\big[e^{-(V_m+28)/5} + 1\big]$

Potassium currents

$I_{KDR} = g_K n^4 (V_m - E_K)$

$\alpha_n = 0.032\big(-(V_m + 63.8)\big)\,/\big[e^{-(V_m+63.8)/5} - 1\big]$

$\beta_n = 0.5e^{-(V_m+68.8)/40}$

$I_{Ks} = g_{Ks} d(0.4e1 + 0.6e2)(V_m - E_K)$

$\tau_d = 2.5 + 0.253/\big(e^{((V_m-81)/25.6)} + e^{(-(V_m+132)/18)}\big)$

$d_\infty = \big[1/1 + e^{-((V_m+43)/17)}\big]^4$

$\tau_{e1} = 30.4 + 0.253/\big(e^{((V_m-1329)/200)} + e^{(-(V_m+130)/7.1)}\big)$

$e1_\infty = 1/1 + e^{((V_m+58)/10.6)}$

$if\ V_m \le -70\ \tau_{e2} = \tau_{e1}; else\ \tau_{e2} = 2260$

$e2_\infty = e1_\infty$

Hyperpolarization activated cation current

$I_h = g_h c^3 (V_m - 43)$

$\tau_c = 1/e^{(-15.45-(0.086V_m))} + e^{(-1.17+0.0701V_m)}$

$c_\infty = 1/e^{(V_m+85)/5.5} + 1$

T-type Ca^{2+} current

$I_T = p_{Ca} m_T^2 h_T G(V_m, Ca_i, Ca_o)$

$$G(V_m, Ca_i, Ca_o) = \left(\frac{z^2F^2V_m}{RT}\right)\left(\frac{Ca_i - Ca_o e^{-zFV_m/RT}}{1 - e^{-zFV_m/RT}}\right)$$

$$\frac{dCa_i}{dt} = \left(\frac{0.00024 - Ca_i}{5}\right) - \frac{I_T k}{zFd}$$

$$\tau_{mT} = 0.204 + 0.333/\left(e^{-((V_m+135)/16.7)} + e^{(V_m+19.8/18.2)}\right)$$

$$mT_\infty = 1/1 + e^{-((V_m+60)/6.2)}$$

$$if\ V_m < -80\ \tau_{hT} = 0.333e^{((V_m+470)/66.6)}$$

$$else\ \tau_{hT} = 9.33 + 0.333e^{-((V_m+25)/10.5)}$$

$$hT_\infty = 1/1 + e^{((V_m+84)/4)}$$

The membrane capacitance C is assumed to be unity, the reversal potentials are $E_{Na} = 45$ mV and $E_K = -95$ mV and the conductances are set to $g_{Na} = 30$, $g_K = 3$, $g_{Ks} = 0.7$, $g_h = 0.5$, $g_{Na,leak} = 0.0207$, $g_{K,leak} = 0.05$ mS/cm^2. For the Ca^{2+} concentration: $k = 5.1821e^{-5}$, $[Ca]_{buf} = 0.00024$ mM, $[Ca]_o = 2$ mM, $\tau_{pump} = 5$ ms, the maximum T-type Ca^{2+} channel permeability $p_{Ca} = 0.1$ cm/s, Z is the charge of a Ca^{2+} ion, F is Faraday's constant in J/(V mol), R is the gas constant in J/(K mol) and T=309.15K.

References

Amirnovin R, Williams ZM, Cosgrove GR, and Eskandar EN. Visually guided movements suppress subthalamic oscillations in Parkinson's disease patients. *Journal of Neuroscience* 24: 11302-11306, 2004.

Anderson ME, Postupna N, and Ruffo M. Effects of High-Frequency Stimulation in the Internal Globus Pallidus on the Activity of Thalamic Neurons in the Awake Monkey. *Journal of Neurophysiology* 89: 1150-1160, 2003.

Benabid AL, Pollak P, Gervason C, Hoffman D, Gao DM, Hommel M, Perret JE, and Rougemont JD. Long-term suppression of tremor by chronic stimulation of the ventral intermediate thalamic nucleus. *Lancet* 337: 403-406, 1991.

Brown P. The oscillatory nature of human basal ganglia activity: relationship to pathophysiology of Parkinson's disease. *Movement Disorders* 18: 357-363, 2003.

Butson CR, and McIntyre CC. Tissue and electrode capacitance reduce neural activation volumes during deep brain stimulation. *Clinical Neurophysiology* 116: 2490-2500, 2005.

Cagnan H, Meijer HGE, van Gils SA, Krupa M, Heida T, Rudolph M, Wadman WJ, and Martens HCF. Thalamic response to frequency: a computational study on clinically effective Deep Brain Stimulation parameters and dynamics of Parkinson's disease. *European Journal of Neuroscience* 30: 1306-1317, 2009.

Carlson JD, Cleary DR, Cetas JS, Heinricher MM, and Burchiel KJ. Deep Brain Stimulation Does Not Silence Neurons in Subthalamic Nucleus in Parkinson's Patients. *Journal of Neurophysiology* 103: 962-967, 2010.

Chen CC, Litvak V, Gilbertson T, Kuhn A, Lu CS, S.T. L, Tsai CH, Tisch S, Limousin P, Hariz M, and Brown P. Excessive synchronization of basal ganglia neurons at 20 Hz slows movement in Parkinson's disease. *Experimental Neurology* 2007.

Chow S-N, and Hale JK. *Methods of bifurcation theory*. New York: Springer-Verlag, 1982.

Coombes S, Owen MR, and Smith GD. Mode locking in a periodically forced integrate-and-fire-or-burst neuron model. *Physical Review E* 64: 419141-4194112, 2001.

Destexhe A, Neubig M, Ulrich D, and Huguenard J. Dendritic low-threshold calcium currents in thalamic relay cells. *Journal of Neuroscience* 18: 3574-3588, 1998.

Destexhe A, and Sejnowski TJ. Interactions between membrane conductances underlying thalamocortical slow-wave oscillations. *Physiological Reviews* 83: 1401-1453, 2003.

Dhooge A, Govaerts W, and Kuznetsov YA. MATCONT:A MATLAB package for numerical bifurcation analysis of ODEs. *ACM Transactions on Mathematical Software* 29: 141-164, 2003.

Dolan K, Martens HCF, Schuurman PR, and Bour LJ. Automatic noise-level detection for extra-cellular micro-electrode recordings. *Medical and Biological Engineering and Computing* 47: 791-800, 2009.

Dostrovsky JO, and Lozano AM. Mechanisms of Deep Brain Stimulation. *Movement Disorders* 17: 63-68, 2002.

Gao DM, Benazzouz A, Piallat B, Bressand K, Ilinsky IA, Kultas-Ilinsky K, and Benabid AL. High-Frequency Stimulation of the Subthalamic Nucleus Suppresses Experimental Resting Tremor in the Monkey. *Neuroscience* 88: 201-212, 1999.

Guo Y, Rubin JE, McIntyre CC, Vitek JL, and Terman D. Thalamocortical relay fidelity varies across subthalamic nucleus deep brain stimulation protocols in a data driven computational model. *Journal of Neurophysiology* 99: 1477-1492, 2008.

Hahn PJ, and McIntyre CC. Modeling shifts in the rate and pattern of subthalamopallidal network activity during deep brain stimulation. *Journal of Computational Neuroscience* 28: 425-441, 2010.

Hahn PJ, Russo GS, Hashimoto T, Miocinovic S, Xu W, McIntyre CC, and Vitek JL. Pallidal burst activity during therapeutic deep brain stimulation. *Experimental Neurology* 211: 243-251, 2008.

Hammond C, Bergman H, and Brown P. Pathological synchronization in Parkinson's disease: networks, models and treatments. *Trends in Neurosciences* 30: 357-364, 2007.

Hashimoto T, Elder CM, Okun MS, Patrick SK, and Vitek JL. Stimulation of the subthalamic nucleus changes the firing pattern of pallidal neurons. *Journal of Neuroscience* 23: 1916-1923, 2003.

Huguenard JR, and McCormick DA. Simulation of the currents involved in rhythmic oscillations in thalamic relay neurons. *Journal of Neurophysiology* 68: 1373-1383, 1992.

Johnson MD, and McIntyre CC. Quantifying the Neural Elements Activated and Inhibited by Globus Pallidus Deep Brain Stimulation. *Journal of Neurophysiology* 100: 2549-2563, 2008.

Johnson MD, Miocinovic S, McIntyre CC, and Vitek JL. Mechanisms and Targets of Deep Brain Stimulation in Movement Disorders. *Neurotherapeutics* 5: 294-308, 2008.

Kim U, Sanchez-Vives MV, and McCormick DA. Functional Dynamics of GABAergic Inhibition in the Thalamus. *Science* 278: 130-134, 1997.

Kuncel AM, Cooper SE, Wolgamuth BR, and Grill WM. Amplitude- and frequency-dependent changes in neuronal regularity parallel changes in tremor with thalamic deep brain stimulation. *IEEE transactions on neural systems and rehabilitation engineering* 15: 190-197, 2007.

Kuznetsov YA. *Elements of Applied Bifurcation Theory*. Berlin: Springer-Verlag, 2004.

Limousin P, Pollak P, Benazzouz A, Hoffmann D, Le Bas JF, Broussolle E, Perret JE, and Benabid AL. Effect on parkinsonian signs and symptoms of bilateral subthalamic nucleus stimulation. *Lancet* 345: 91-95, 1995.

Lozano AM, Dostrovsky JO, Chen R, and Ashby P. Deep Brain stimulation for Parkinsons disease: distrupting the disruption. *Lancet Neurology* 1: 225-231, 2002.

Magill PJ, Bolam JP, and Bevan MD. Relationship of activity in the subthalamic nucleus-globus pallidus network to cortical electroencephalogram. *Journal of Neuroscience* 20: 820-833, 2000.

Magnin M, Morel A, and Jeanmonod D. Single-unit analysis of the pallidum, thalamus, and subthalamic nucleus in parkinsonian patients. *Neuroscience* 96: 549-564, 2000.

McCormick DA, and Huguenard JR. A model of the electrophysiological properties of thalamocortical relay neurons. *Journal of Neurophysiology* 68: 1384-1400, 1992.

McIntyre CC, Grill WM, Sherman DL, and Thakor NV. Cellular Effects of Deep Brain Stimulation: Model-Based Analysis of Activation and Inhibition. *Journal of Neurophysiology* 91: 1457-1469, 2004.

Molnar GF, Pilliar A, Lozano AM, and Dostrovsky JO. Differences in Neuronal Firing Rates in Pallidal and Cerebellar Receiving Areas of Thalamus in Patients With Parkinson's Disease, Essential Tremor, and Pain. *Journal of Neurophysiology* 93: 3094-3101, 2005.

Moro E, Esselink RJA, Xie J, Hommel M, Benabid AL, and Pollak P. The impact on Parkinson's disease of electrical parameter settings in STN stimulation. *Neurology* 59: 706-713, 2002.

Moroney R, Heida C, and Geelen J. Increased bradykinesia in Parkinson's disease with increased movement complexity: elbow flexion-extension movements. *Journal of Computational Neuroscience* 25: 501-519, 2008.

Nini A, Feingold A, Slovin H, and Bergman H. Neurons in the globus pallidus do not show correlated activity in the normal monkey, but phase-locked oscillations appear in the MPTP model of parkinsonism. *Journal of Neurophysiology* 74: 1800-1805, 1995.

Raz A, Vaadia E, and Bergman H. Firing patterns and correlations of spontaneous discharge of pallidal neurons in the normal and tremulous 1-methyl-4-phenyl-1,2,3,6 tetrahydropyridine vervet model of Parkinsonism. *Journal of Neuroscience* 20: 8559-8571, 2000.

Reese R, Steigerwald F, P\"otter M, Herzog J, Deuschl G, Volkmann J, Pinsker MO, and Mehdorn HM. High-frequency stimulation of the subthalamic nucleus increases pallidal neuronal firing rate in a patient with Parkinson's disease. *Movement Disorders* 23: 1945-1947, 2008.

Rizzone M, Lanotte M, Bergamasco B, Tavella A, Torre E, Faccani G, Melcarne A, and Lopiano L. Deep brain

stimulation of the subthalamic nucleus in Parkinson's disease: effects of variation in stimulation parameters. *Journal of Neurology Neurosurgery and Psychiatry* 71: 215-219, 2001.

Rubin JE, and Terman D. High Frequency Stimulation of the Subthalamic Nucleus Eliminates Pathological Thalamic Rhythmicity in a Computational Model. *Journal of Computational Neuroscience* 16: 211-235, 2004.

Sherman SM. Tonic and burst firing: Dual modes of thalamocortical relay. *Trends in Neurosciences* 24: 122-126, 2001.

Smith GD, Cox CL, Sherman SM, and Rinzel J. A firing-rate model of spike-frequency adaptation in sinusoidally-driven thalamocortical relay neurons. *Thalamus and Related Systems* 1: 135-156, 2001.

Smith GD, Cox CL, Sherman SM, and Rinzel J. Fourier Analysis of Sinusoidally Driven Thalamocortical Relay Neurons and a Minimal Integrate and Fire or Burst Model. *Journal of Neurophysiology* 83: 588-610, 2000.

Smith Y, Bevan MD, Shink E, and Bolam JP. Microcircuitry of the Direct and Indirect pathways of the Basal Ganglia. *Neuroscience* 86: 353-387, 1998.

Temperli P, Ghika J, Villemure J-G, Burkhard PR, Bogousslavsky J, and Vingerhoets FJG. How do parkinsonian signs return after discontinuation of subthalamic DBS? *Neurology* 60: 78-81, 2003.

Terman D, Rubin JE, Yew AC, and Wilson CJ. Activity Patters in a Model for the Subthalamopallidal Network of the Basal Ganglia. *Journal of Neuroscience* 22: 2963-2976, 2002.

Trottenberg T, Kupsch A, Schneider GH, Brown P, and Kuhn AA. Frequency dependent distribution of local field potential activity within the subthalamic nucleus in Parkinson's disease. *Experimental Neurology* 2007.

Volkmann J, Herzog J, Kopper F, and Geuschl G. Introduction to the programming of deep brain stimulators. *Movement Disorders* 17: S181-S187, 2002.

Volkmann J, Moro E, and Pahwa R. Basic algorithms for the programming of deep brain stimulation in Parkinson's disease. *Movement Disorders* 21: S284-S289, 2006.